Multifunctional Phosphorescent Conjugated Polymer Nanoparticles for Reactive Oxygen Species Generation and Imaging Applications

ZHAO Yanli
Division of Chemistry and Biological Chemistry
School of Physical and Mathematical Sciences
Nanyang Technological University
S637371
Singapore
zhaoyanli@ntu.edu.sg

KWOK Ling Yi Samantha* and SOH Hui Ling*
Raffles Science Institute
Raffles Institution
S575954
Singapore
* These authors contributed equally to this work.

***Abstract*—Classical photodynamic therapy (PDT) suffers from drawbacks. Insufficient tumour selectivity increases toxicity risks and limits photosensitiser concentration in the tumour, resulting in low therapeutic efficacy. Hence, nanoparticles are important to confer greater selectivity. However, separate component polymeric nanocarrier systems with encapsulated photosensitisers have less than optimal energy transfer efficiency due to the larger distance between the donor and acceptor. This project thus aims to synthesise a single component photosensitiser platform for PDT and imaging applications.**

Polyfluorenes containing iridium complexes (PFO-Ir) comprise a polymer backbone covalently bonded to iridium complexes. PFO-Ir is a desirable candidate for fabricating nanoparticles due to its high triplet state energy level and ability to function as both photosensitiser and imaging agent. PEG-coated and uncoated PFO-Ir12 nanoparticles were synthesised through nanoprecipitation and characterized subsequently. Their reactive oxygen species generation abilities were then determined and compared through the quenching of ADMA. The nanoparticle uptake by HeLa cells was explored through confocal imaging.

Morphological characterisation indicated that nanoprecipitation forms spherical and monodisperse PFO and PFO-Ir12 nanoparticles. In addition, the results showed that uncoated PFO-Ir12 nanoparticles had more efficient reactive oxygen species production. Interestingly, this study also found that PFO-Ir12 nanoparticles had a greater than expected formation and/ or stability of the β-phase of the PFO main chain, which may be attributed to the formation of nanoparticles. This resultant increased energy transfer can potentially improve the efficiency of current photoactivable systems. PFO-Ir12 nanoparticles are one of the first single component nanoplatforms to be synthesized and characterized for PDT and imaging applications.

Keywords-Photodynamic therapy; imaging; photosensitiser; polymer; nanoparticles

I. INTRODUCTION

Recent trends have shown a shift in focus from conventional nanoplatforms activated by internal biological stimuli to those by external stimuli. The latter offers greater spatio-temporal precision that not only augments the curative potential of treatments, but also minimises the adverse systemic side effects [1-3]. An external stimulus is light. Conferring high precision and minimal invasiveness [4], the application of light in photodynamic therapy (PDT) for cancer treatment is of high interest.

A typical PDT system involves photosensitisers, molecular oxygen, and light [5]. The excitation of a photosensitiser by light of a specific wavelength leads to energy transfer to molecular oxygen, a process which generates singlet oxygen [6]. Singlet oxygen is extremely cytotoxic and has a limited in vivo lifetime [7], thus resulting in a small region of action. This allows PDT to be effective in its application to a cancerous region while leaving healthy tissues unscathed [8-10]. However, classical PDT suffers from drawbacks that limit its effectiveness. For instance, insufficient tumour selectivity of current clinically accepted photosensitisers not only increases the risk of systemic toxicity, but also limits photosensitiser concentration in the tumour, resulting in low therapeutic efficacy [11]. Hence, the involvement of nanoparticles is important to confer higher tumour selectivity [5].

Particularly, π-conjugated polymer nanoparticles (CPNPs) present multifarious advantages such as their biocompatible nature, small size, and excellent optoelectronic properties including large Stokes shift, high fluorescent brightness, fast energy transfer and superior photostability [12-15]. Conjugated phosphorescent polyfluorenes containing iridium complexes (PFO-Ir) have been reported to be effective electroluminescent materials [16]. Furthermore, the presence of an efficient energy transfer from the polymer main chain to the Ir(III) complex has been reported. This energy can then be transferred from the excited electrons of the phosphorescent Ir(III) complex to electrons in the ground state of molecular oxygen, making Ir(III) a suitable photosensitiser [17]. PFO is highly suitable as the host material due to its high triplet state energy level and outstanding charge-transport characteristics [18]. Hence, PFO-Ir was selected for the synthesis of nanoparticles for PDT.

Specifically, PFO-Ir with a feed ratio of Ir(III) complex of 12% (PFO-Ir12) was chosen. The β-phase of PFO, which can be aggregation-induced, is more ordered than α-phase and increases energy transfer from PFO to the photosensitiser. A stable β-phase is less easily formed at higher Ir(III) content [19]. This may be due to increased steric hindrance and/or shortened PFO segments, resulting in increased aggregation difficulty. Nonetheless, PFO-Ir12 was chosen over PFO-Ir

polymers with lower Ir(III) content as the higher amounts of photosensitisers present in PFO-Ir12 nanoparticles may confer greater reactive oxygen species (ROS) production ability.

Apart from their usage in PDT, Ir(III) complexes, endowed with the advantages of visible excitation and long fluorescence lifetime [20-21], can be utilised for imaging. The long fluorescence lifetime may allow the disregarding of autofluorescent background interferences without impairing tissue integrity [22]. Coupled with the propensity of nanoparticles to accumulate in tumours due to the enhanced permeability and retention effect, PFO-Ir12 nanoparticles are suitable for generating a fluorescence contrast to delimit the margin separating cancerous from healthy tissues, which is imperative in treatment modalities. This further supports the usage of PFO-Ir12 nanoparticles for the multiplexing of imaging and therapeutic applications [23].

In this study, PEG-coated and uncoated PFO-Ir12 nanoparticles were synthesised using a modified nanoprecipitation method. Morphological characterisation was done using high resolution transmission electron microscopy (HR-TEM) and dynamic light scattering (DLS), and compared with that of PFO nanoparticles. The photophysical properties of PFO and PFO-Ir12 nanoparticles were elucidated through UV-visible absorption and photoluminescence (PL) spectroscopies. Their reactive oxygen species (ROS) generation abilities under light irradiation were then compared. Finally, the applicability of PFO-Ir12 nanoparticles for imaging and PDT was explored through confocal laser scanning microscopy (CLSM) of HeLa (human cervical carcinoma) cells.

Presently, photoexcited by 405 nm light, PFO-Ir12 nanoparticles may be applied for the treatment of body regions similar to that of the few currently approved photosensitisers activable at wavelengths of 375 nm – 405 nm, such as 5-aminolevulinic acid (5-ALA) and 5-aminolevulinic acid hexelesther (5-ALA hexelesther) [5]. Most importantly, PFO-Ir12 nanoparticles utilise one of the first single component photosensitisers, as opposed to conventional photosensitizer nanoplatforms with multiple components [11]. This allows for greater energy transfer efficiency. Hence, this study aims to synthesise and further optimise a PDT nanoplatform based on PFO-Ir12 nanoparticles to provide insight on the future development of treatment modalities.

II. Materials And Methods

A. Chemical Structures of PFO and PFO-Ir12 Polymers

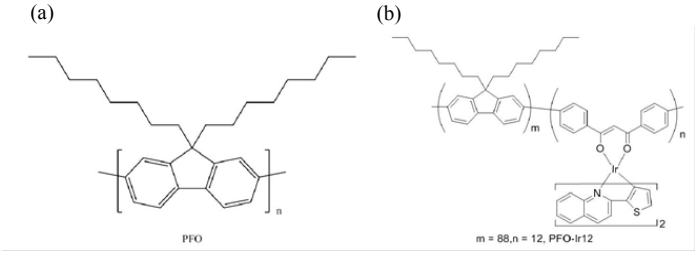

Figure 1. Chemical structures of (a) PFO polymer and (b) PFO-Ir12 polymer

B. Synthesis of polymers

PFO was synthesised according to Feng et al. (2010) [24] and PFO-Ir12, Shi et al. (2010) [19].

C. Preparation of PFO Nanoparticles through Nanoprecipitation

A tetrahydrofuran (THF; Sigma Aldrich 401757) solution of PFO (1.0 mg/mL, 0.25 mL) was added dropwise to an aqueous solution of poly(ethylene glycol) methyl ether (PEG) (1% w/v, 2mL; Sigma Aldrich) under moderate stirring (500 rpm). The solution was stirred overnight at 500 rpm to ensure complete organic phase evaporation. The nanoparticles were recovered through centrifugation at 14800 rpm for 15 minutes (Satorius Sigma 1-14, UK) and washed with deionised water.

D. Preparation of PFO-Ir12 Nanoparticles through Nanoprecipitation

A THF solution of PFO-Ir12 (2.0 mg/mL, 1 mL) was added dropwise to an aqueous PEG solution (0.25% w/v, 5 mL) under vigorous stirring (1000 rpm). The mixture was then stirred for 2 hours at 1000 rpm. The PEG-coated PFO-Ir12 nanoparticles were recovered through centrifugation at 14800 rpm for 15 minutes. Uncoated PFO-Ir12 nanoparticles were prepared using 5 mL of deionised water as the aqueous phase. All other factors were kept constant.

E. Characterisation of PFO and PFO-Ir12 Nanoparticles

Diluted suspensions of nanoparticles were left to dry overnight on TEM sample grids. HR-TEM images were then taken at an accelerating voltage of 200 kV (EOL 2010 TEM). The hydrodynamic diameters of the nanoparticles were also analysed using particle sizing software (90 plus, Brookhaven Instruments Co. USA) through DLS, at a fixed angle of 90° at room temperature. The PL spectra of the nanoparticles were measured using Shimadzu RF5300 with Xe lamp excitation source and Edinburgh FL 920 instrument. A UV-3600 Shimadzu UV-Vis spectrophotometer was used to record the UV-Vis absorption spectra.

F. Reactive Oxygen Species (ROS) Generation in Solution

The singlet oxygen generation abilities of the PFO-Ir12 nanoparticles were measured by detecting the absorption spectral changes of 2,2-(anthracene-9,10-diylbis(methylene))dimalonic acid (ADMA). 2 ml of 10 mM phosphate buffered saline (PBS) solution (Sigma Aldrich P3813) was added into a quartz cuvette along with 50 µl of 2 M ADMA solution (Sigma Aldrich). The absorption spectra were recorded between five minute intervals of irradiation at 405 nm.

G. Cellular Imaging

HeLa cells were seeded in a 6-well plate (NUNC) at 2 x 10^4 cells/cm^{-2}. 24 hours later, cell culture media was changed to that with 15 µM of PFO-Ir12. 12 hours later, media was removed and the cells were washed with PBS buffer (pH=7.4). Cells were fixed with 4.0 % formaldehyde (1 mL), followed

by washing with PBS buffer thrice. Subsequently, confocal microscopy images were taken using a Leica TCS confocal microscope (Nikon, Eclipse TE2000-E, 60x oil objective) with 405 nm light.

III. Results And Discussion

A. Morphological Characterisation of PFO and PFO-Ir12 Nanoparticles

Morphological characterisation by HR-TEM and DLS indicate that nanoprecipitation allows for formation of PFO and PFO-Ir12 nanoparticles that are spherical and monodisperse. From the TEM images, the average sizes of both PFO and PEG-coated PFO-Ir12 nanoparticles were about 50 nm (Figures 2a and 2b). The hydrodynamic diameters as measured by DLS were larger than those estimated from TEM images, 72.8 nm and 54.3 nm for PFO and PEG-coated PFO-Ir12 nanoparticles respectively, due to a layer of solvent coating the nanoparticles (Figures 3a and 3b). Comparison of the morphologies of PFO and PFO-Ir12 nanoparticles shows that despite the higher iridium content and shorter PFO main chain in PFO-Ir12, the morphology was not negatively affected.

The effect of PEG on the size of PFO-Ir12 nanoparticles was also investigated. When deionised water was used as the aqueous phase, the average size of the uncoated PFO-Ir12 nanoparticles was about 25 nm (Figure 2c). The comparatively larger size of about 50 nm of the PEG-coated PFO-Ir12 nanoparticles may be due to the presence of surfactant coating the outer surface of the nanoparticles (Figure 2b).

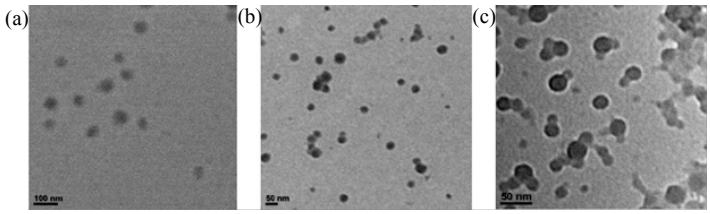

Figure 2. Transmission electron micrographs of a) PFO nanoparticles, b) PEG-coated PFO-Ir12 nanoparticles and c) uncoated PFO-Ir12 nanoparticles

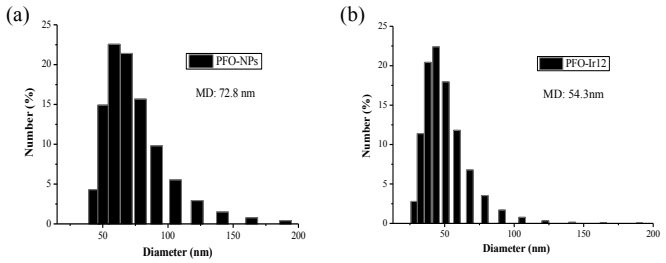

Figure 3. Size distribution of a) PFO nanoparticles and b) PFO-Ir12 nanoparticles

B. Photophysical Characterisation and Comparison of PFO and PFO-Ir12 Nanoparticles

1) Absorption Spectra of PFO and PFO-Ir12 Nanoparticle

A main absorption band centered at around 380 nm was observed for both PFO and PFO-Ir12 nanoparticles in aqueous solution (15 μM) (Figures 4a and 4b). This was due to the promotion of electrons from π bonding orbitals to π* antibonding orbitals of the PFO polymer main chain. This implies that the irradiation for PDT would be most efficient near 380 nm.

In addition, a small shoulder at 435 nm and 425 nm was observed for PFO and PFO-Ir12 nanoparticles respectively. These shoulders are attributable to the β-phase of the polymer main chain. While PFO nanoparticles have been previously reported to exhibit β-phase, this is a surprising finding for PFO-Ir12 nanoparticles. According to Shi et al. (2011), the intensity of the β-phase drops significantly as the feed ratio of iridium complexes increases from 2% in PFO-Ir2 to 8% in PFO-Ir8 polymer, to the extent that the β-phase for the PFO-Ir12 free polymer should be almost negligible [18]. However, PFO-Ir12 nanoparticles have a greater than expected formation and/ or stability of the β-phase of the PFO main chain. The formation of nanoparticles may account for this. The β-phase may increase energy transfer from PFO to the photosensitiser due to the higher triplet energy of the β-phase than that of the Ir(III) complex [25-26] and greater spectral overlap of the emission of the β-phase of the PFO main chain with the absorption of the Ir(III) complex as compared to α-phase due to the redshift, in accordance to the Förster energy-transfer (FRET) mechanism [27]. The fraction of β-phase also impacts the photoluminescence quantum efficiency [28-29]. A weak absorption band observed around 450–550 nm was due to the metal-to-ligand charge-transfer transition of the Ir(III) complex (Figure 4b).

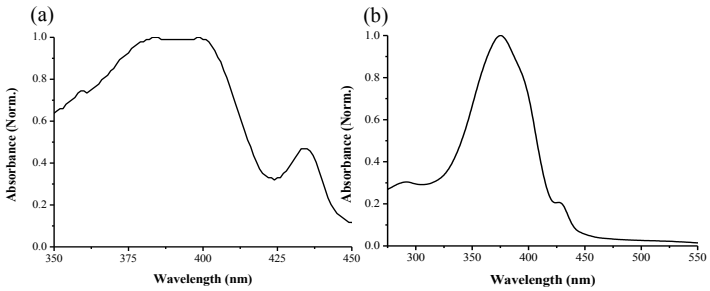

Figure 4. Absorption spectra of a) PFO nanoparticles and b) PFO-Ir12 nanoparticles

2) Photoluminescence Spectra of PFO and PFO-Ir12 nanoparticles

In the PL spectra, emission peaks occurred at 435 nm and 465 nm due to the polyfluorene main chain for both PFO and PFO-Ir12 nanoparticles (Figure 5a and 5b). Additionally, a major red emission peak occurred at 620 nm for PFO-Ir12 nanoparticles due to the phosphorescent Ir(III) complex (Figure 5b).

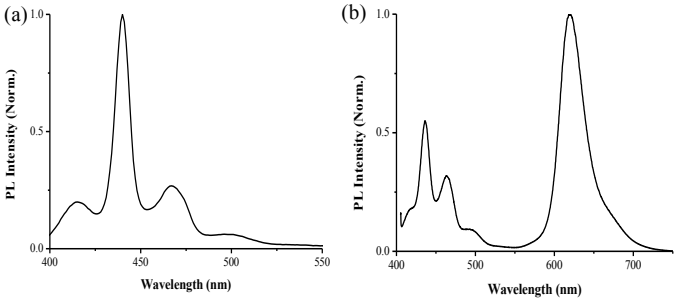

Figure 5. Photoluminescence spectra of a) PFO nanoparticles and b) PFO-Ir12 nanoparticles

C. *Reactive Oxygen Species Generation*

ADMA was utilized to capture singlet oxygen photogenerated by PFO-Ir12 nanoparticles. The resultant absorption spectral quenching of ADMA was tracked at 259 nm. Upon excitation of both uncoated and PEG-coated PFO-Ir12 nanoparticles with 405 nm light, the absorbance at 259 nm (ADMA) decreased continuously, while the absorbance at 375 nm (PFO-Ir12 nanoparticles) varied negligibly (Figures 6a and 6b). This demonstrates ROS generation and low photobleaching.

In addition, the logarithms of the ratios of absorbance at 259 nm to that at 375 nm were plotted against irradiation time (Figure 7). An exponential relationship was observed. A more negative gradient associated with uncoated PFO-Ir12 indicated a significantly higher ROS generation rate. This may be because the PEG coating of the PEG-coated nanoparticles interfered with the access of the iridium complexes to molecular oxygen and delayed the release of singlet oxygen into the PBS solution. This suggests that although PEG can be used to improve biocompatibility, it reduces the ROS generation efficiency.

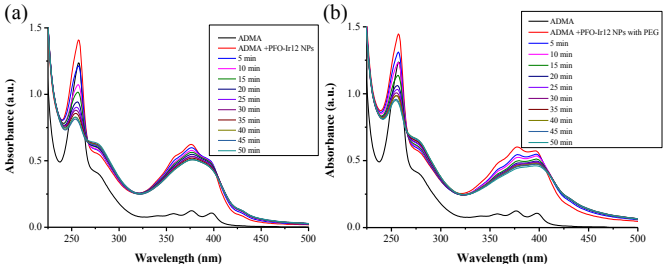

Figure 6. Absorption spectra of ADMA only and ADMA with a) uncoated PFO-Ir12 / b) PEG-coated PFO-Ir12 irradiated at 405nm for every 5 minute interval for a total duration of 50 minutes

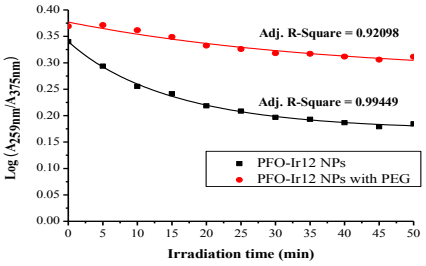

Figure 7. Graph of the function log (A_{259nm} / A_{375nm}) against irradiation time

D. *Cellular Imaging*

The blue emission observed at 420–460 nm was attributed to fluorescence from the PFO main chain (Figure 8a), while the red emission at 600–650 nm was ascribed to the Ir(III) complex (Figure 8b). Both the blue and red luminescence can be seen in the cells' cytoplasm in the overlay image, indicating that PFO-Ir12 nanoparticles were endocytosed by the cells (Figure 8c). This shows that PFO-Ir12 nanoparticles are suitable for intracellular delivery. Confocal imaging of the HeLa cells also shows that PFO-Ir12 nanoparticles can act as an imaging agent which fluoresces upon excitation with 405 nm light to produce visible light. This allows PFO-Ir12 nanoparticles to be used for photosensitiser fluorescence detection and in dosimetry [30-33].

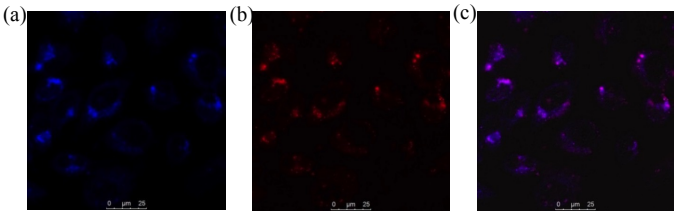

Figure 8. Images of HeLa cells from confocal laser scanning microscopy (CLSM) observed at a) 420–460 nm and b) 600–650 nm and c) overlay image of (a) and (b)

IV. Conclusion

In summary, a novel single component nanoplatform for imaging and ROS production based on phosphorescent PFO-Ir12 nanoparticles was synthesised and characterised. In addition, while PEG may improve the biocompatibility of the nanoparticles, it reduces the efficiency of reactive oxygen species generation. Furthermore, this study established that nanoparticles may have a greater formation and/or stability of β-phase as compared to free polymers. This can contribute to improving the energy transfer efficiency of current PDT systems, leading to a reduction in the amount of radiation required, thereby minimising the negative side effects of therapy. In this study, the measurement of ROS generation was conducted in solution. In future studies, ROS generation can be measured in vitro and in vivo to explore the treatment efficacy. Although the current study is limited by less optimal tissue penetration ability due to the usage of 405 nm light, this can be addressed by encapsulating upconverting nanoparticles (UCNPs) within PFO-Ir12 nanoparticles. This way, near-infrared light with better tissue penetration abilities can be converted to visible light to excite the PFO-Ir system.

Acknowledgment

The authors would like to express their heartfelt gratitude to Nanyang Technological University (NTU) for supporting this project, Assistant Professor Zhao Yanli and Dr Shi Huifang (SPMS-CBC) for their invaluable guidance throughout this project.

REFERENCES

[1] Timko, B., Dvir, T., & Kohane, D. (2010). Remotely Triggerable Drug Delivery Systems.Advanced Materials, 22(44), 4925-4943.

[2] Roy, D., Cambre, J., & Sumerlin, B. (2010). Future perspectives and recent advances in stimuli-responsive materials. Progress in Polymer Science, 35(1-2), 278–301.

[3] Cohen Stuart, M., Huck, W., Genzer, J., Müller, M., Ober, C., Stamm, M., ... Minko, S. (n.d.). Emerging Applications Of Stimuli-responsive Polymer Materials. Nature Materials, 9, 101-113.

[4] Gohy, J., & Zhao, Y. (2013). Photo-responsive block copolymer micelles: Design and behavior. Chemical Society Reviews, 24(17), 7117-7129.

[5] Monge-Fuentes, V., Alexandre Muehlmann, L., & Bentes de Azevedo, R. (2014). Perspectives on the application of nanotechnology in photodynamic therapy for the treatment of melanoma. Nano Reviews, 5.

[6] Dougherty, T., Gomer, C., Henderson, B., Jori, G., Kessel, D., Korbelik, M., ... Qian, P. (1998). Photodynamic Therapy. Journal of the National Cancer Institute, 9(12), 889-905.

[7] Moan, J., & Berg, K. (n.d.). The Photodegradation Of Porphyrins In Cells Can Be Used To Estimate The Lifetime Of Singlet Oxygen. Photochemistry and Photobiology, 53(4), 549-553.

[8] Wang, C., Cheng, L., Liu, Y., Wang, X., Ma, X., Deng, Z., ... Liu, Z. (2013). Imaging-Guided pH-Sensitive Photodynamic Therapy Using Charge Reversible Upconversion Nanoparticles under Near-Infrared Light. Advanced Functional Materials, 23(24), 3077-3086.

[9] Zhang, Y., Qian, J., Wang, D., Wang, Y., & He, S. (2012). Multifunctional Gold Nanorods with Ultrahigh Stability and Tunability for In Vivo Fluorescence Imaging, SERS Detection, and Photodynamic Therapy. Angewandte Chemie International Edition, 52(4), 1148-1151.

[10] Shibu, E., Hamada, M., Murase, N., & Biju, V. (2013). Nanomaterials formulations for photothermal and photodynamic therapy of cancer. Journal of Photochemistry and Photobiology C: Photochemistry Reviews, 15, 53-72.

[11] D, K. (1992). Photodynamic Therapy of Neoplastic Disease. Oncol Res, 4(6), 219-225.

[12] Jiang, H., Taranekar, P., Reynolds, J., & Schanze, K. (2009). Conjugated Polyelectrolytes: Synthesis, Photophysics, and Applications. Angewandte Chemie International Edition,48(24), 4300-4316.

[13] Pu, K., & Liu, B. (2011). Fluorescent Conjugated Polyelectrolytes for Bioimaging. Advanced Functional Materials, 21(18), 3408-3423.

[14] Zhu, C., Liu, L., Yang, Q., Lv, F., & Wang, S. (2012). Water-Soluble Conjugated Polymers for Imaging, Diagnosis, and Therapy. Chemical Reviews, 112(8), 4687-4735.

[15] Feng, L., Liu, L., Lv, F., Banzan, G., & Wang, S. (2014). Preparation and Biofunctionalization of Multicolor Conjugated Polymer Nanoparticles for Imaging and Detection of Tumor Cells. Advanced Materials, 26(23), 3926–3930.

[16] Keshtov, M., Maltsev, E., Marochkin, D., Lypenko, D., Kuklin, S., Smol'yakova, A., & Khokhlov, A. (2013). Synthesis and Optoelectronic Properties of Conjugated Phosphorescent Copolyfluorenes Containing Iridium Complexes in Main Chains and Light-Emitting Diodes Formed on Their Basis. Polymer Science Series B, 56(1), 77-88.

[17] Shi, H., Ma, X., Zhao, Q., Liu, B., Qu, Q., An, Z., ... Huang, W. (2013). Ultrasmall Phosphorescent Polymer Dots for Ratiometric Oxygen Sensing and Photodynamic Cancer Therapy. Advanced Functional Materials, 24(30), 4823–4830.

[18] Shi, H., Nakai, Y., Liu, S., Zhao, Q., An, Z., Tsuboi, T., & Huang, W. (2011). Improved Energy Transfer through the Formation of the β Phase for Polyfluorenes Containing Phosphorescent Iridium(III) Complexes. The Journal of Physical Chemistry C, 115(23), 11749–11757.

[19] Shi, H., Liu, S., Sun, H., Xu, W., An, Z., Chen, J., Huang, W. (2010). Simple Conjugated Polymers with On-Chain Phosphorescent Iridium(III) Complexes: Toward Ratiometric Chemodosimeters for Detecting Trace Amounts of Mercury(II). Chemistry - A European Journal, 12158-12167.

[20] Zhao, Q., Li, F., & Huang, C. (2010). Phosphorescent chemosensors based on heavy-metal complexes. Chemical Society Reviews, 3007-3007.

[21] Wong, W., & Ho, C. (2009). Heavy metal organometallic electrophosphors derived from multi-component chromophores. Coordination Chemistry Reviews, 253(13-14), 1709–1758

[22] Oliveira VC1, Carrara RC, Simoes DL, Saggioro FP, Carlotti CG Jr, Covas DT, Neder L. (2010). Sudan Black B treatment reduces autofluorescence and improves resolution of in situ hybridization specific fluorescent signals of brain sections. Journal of Histology & Histopathology, 25(8).

[23] Celli, J., Spring, B., Rizvi, I., Evans, C., Samkoe, K., Verma, S., ... Hasan, T. (2010). Imaging and Photodynamic Therapy: Mechanisms, Monitoring, and Optimization. Chemical Reviews,2795-2838.

[24] Feng, X., Lv, F., Liu, L., Tang, H., Xing, C., Yang, Q., & Wang, S. (2010). Conjugated Polymer Nanoparticles for Drug Delivery and Imaging. ACS Applied Materials & Interfaces, 2(8), 2429-2435.

[25] Zhao, Q., Liu, S., & Huang, W. (2010). Promising Optoelectronic Materials: Polymers Containing Phosphorescent Iridium(III) Complexes. Macromolecular Rapid Communications, 31(9-10), 794-807.

[26] Liu, S., Zhao, Q., Mi, B., Huang, W. (2008). Polyfluorenes with On-Chain Metal Centers. Advances in Polymer Science, 125-144.

[27] Gong, X., Ostrowski, J., Moses, D., Bazan, G., & Heeger, A. (2003). Electrophosphorescence from a Polymer Guest–Host System with an Iridium Complex as Guest: Förster Energy Transfer and Charge Trapping. Advanced Functional Materials, 13(6), 439-444.

[28] Cadby, A., Lane, P., Mellor, H., Martin, S., Grell, M., Giebeler, C., ... Vardeny, Z. (2000). Film morphology and photophysics of polyfluorene. Physical Review B, 62(23), 15604-15609.

[29] Wu, C., & Mcneill, J. (2008). Swelling-Controlled Polymer Phase and Fluorescence Properties of Polyfluorene Nanoparticles. Langmuir, 24(11), 5855-5861.

[30] Koo, Y., Fan, W., Hah, H., Xu, H., Orringer, D., Ross, B., ... Kopelman, R. (2007). Photonic explorers based on multifunctional nanoplatforms for biosensing and photodynamic therapy. Applied Optics, 46(10), 1924-1930.

[31] Mccarthy, J., & Weissleder, R. (2008). Multifunctional magnetic nanoparticles for targeted imaging and therapy. Advanced Drug Delivery Reviews, 60(11), 1241-1251.

[32] Pandey, S., Gryshuk, A., Sajjad, M., Zheng, X., Chen, Y., Abouzeid, M., ... Pandey, R. (2005). Multimodality Agents for Tumor Imaging (PET, Fluorescence) and Photodynamic Therapy. A Possible "See and Treat" Approach. Journal of Medicinal Chemistry, 48(20), 6286-6295.

[33] Reddy, G., Bhojani, M., Mcconville, P., Moody, J., Moffat, B., Hall, D., ... Ross, B. (2006). Vascular Targeted Nanoparticles for Imaging and Treatment of Brain Tumors. Clinical Cancer Research, 12(22), 6677-6686.